A novel analysis of oil-film flow visualisations on swept wings

Shanying Zhang* and John T Turner

School of Mechanical, Aerospace and Civil Engineering, University of Manchester, M13 9PL, U.K.
*corresponding author: Shanying.zhang@manchester.ac.uk

Abstract Comparing with static images, video clips of the oil-film surface visualisation enable flow patterns to be monitored during its formation and interpreted more clearly and accurately. Using successive images extracted from the video of flow visualisation, the movement of the oil pigment has been estimated using cross-correlation between nearby image frames after a series of post-processing procedures. This method has been proved to be useful in obtaining the correct directions of the surface skin friction and also indication of their strength.

Using this technique, flow over moderately swept wings, characterised by complex localised flow vortex topologies, have been studied. Two models of complex cambered, twisted, tapered wings with 40 and 60 degree leading edge sweep were investigated at a range of Reynolds number from 2.1×105 to 8.4×105 and range of incidence angles. The influence of the incidence angle was discussed through analysing flow pattern over the wing surface. Comparison of results has been made between the post-processing of oil-film flow visualisations and laser Doppler measurements at 0.2 mm near the surface, and shows a reasonable agreement. Besides, quantitative analysis of oil-film visualisation was conducted and useful information has been obtained in this study.

Keywords: flow visualisation, oil-film flow visualisation, swept wing

1 Introduction

Oil-film flow visualisation is a traditional technique to investigate flow over solid surface, and provides qualitative information about the flow topologies or indication of the complex flow structures. Due to its simplicity, this technique was implemented at the beginning of the wind tunnel testing history. Haines [1] made a range of tests on swept-back wings at high incidence and low Mach number using this technique. Later, flow structures over a tapered swept back wing were investigated at a few higher Mach numbers by Hall and Rogers [2, 3]. Modern digital techniques have rejuvenated this flow diagnostics for broader applications. A brief review on its application on separated flow can be found in Lu [4]. Tanner and Blows [5] applied oil films to measure skin friction and new development on extraction of the skin-friction have been discussed in Liu [6]. The critical point theory is commonly used to interpret the three-dimensional separated flow [7]. By using the concepts of skin friction lines, critical points, separation lines and separated sheets the flow topology can be described consistently.

However, the interpretation of the oil-film visualisation results can be difficult and need some skills, experience or other assistant. Sometime, it is insufficient to allow the correct interpretation of flow directions and strength of the skin friction. The final visualisation pictures can be very misleading without referring to other related information, especially for complex flow patterns with reverse flows at the surface. When the instantaneous video images are not sufficiently clear to show the movement of the oil pigment, cross-correlation between adjacent video frames can be carried out to provide more information on the velocity field over the surface

Turner and Zhang [8] show an example result of the cross-correction of the visualisation video frames for the first time. In the present paper, the emphasis is given to the detailed technique on this novel analysis of oil-film visualisation although a range of other techniques, such as laser Doppler anemometry (LDA), particle image velocimetry (PIV) and force and moment balance, have been used in the investigation of the flow over two swept wing models. The time-averaged three-component velocity results over swept wing models using three-component laser Doppler anemometry (LDA) can be found in Zhang et. al[9].

In the next part, experimental arrangement will be introduced briefly. Then, the detailed data processing procedure, including pre-processing, cross-correlation and post-processing, will be described before the main results were explained with some discussions. Finally, the main findings and the future work will be summarised in the conclusion.

2. Experimental Apparatus

Two swept wing models with swept angles of 40 and 60 degree were tested in the Avro Wind Tunnel at the Goldstein Laboratory, University of Manchester. The working section of this general-purpose, closed-return wind tunnel is nominally rectangular: 2.7 m in width and 2.2 m in height with corner fillets. The length of the working section is about 4m. The upstream settling chamber, incorporating a honeycomb and damping screens to optimise the flow distribution and reduce the turbulence levels in the working section, was followed by an inlet contraction with an area ratio of 6:1. This arrangement produced relatively low free-stream turbulence levels, remaining below 1% for velocities in the range 10 to 60 ms^{-1}.

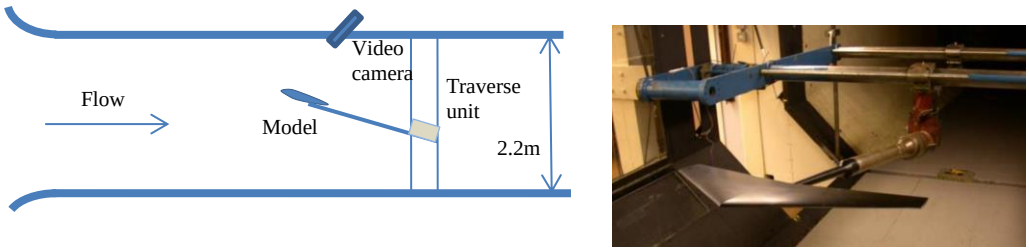

Figure 1: Overall layout and picture of the test section with swept wing model

Two symmetrical full-span wing models were machined from solid aluminium, without a fuselage. The 40° swept wing model had a full span of 650 mm, a root chord of 303·3 mm and a tip chord of 90·9 mm, with a constant 6% thickness to chord ratio along the whole span. This relatively sophisticated wing model was twisted around its straight trailing edge, producing a kink in the leading-edge. The 60° swept wing model also had a full span of 650 mm, a root chord of 685 mm and a tip chord of 10 mm, with a constant 4% thickness to chord ratio along the whole span. The swept wing models were supported by a 1.5 m long sting pointing upstream into the flow, as shown in Figure 1. A mechanical traversing mechanism was used to control the swept wing model remotely in pitch, yaw, and roll. With this arrangement, the apex of the model was considered to be sufficiently far upstream of the traversing mechanism for any blockage effects associated with the model support to be ignored.

A mixture of fluorescent paint pigment and paraffin at the ratio of about 1:5 was chosen in the visualisation of surface flow after trial-and-error. The mixture was brushed evenly onto the suction surface of the swept wing models and the tunnel was run at a fixed speed until the paraffin was evaporated or blown off, leaving the flow pattern record. This technique usually affected by several factors, such as uniformity and density of the paint pigment, the size of the oil pigment particle. Also, rough surface can trigger flow transition from laminar to turbulent to happen earlier.

Sony Handycam 560x camera was mounted on the ceiling of the working section, and normal to the wing model for recording the movement of the oil pigment at the surface. Colour videos, which sampled at 25 frames per second with resolution of 720×576 pixels, were recorded, and then transferred to computer via S–video cable for further analysis.

3. Data Processing

A series of image frames with a time interval of 0.04 second were extracted from the video at a sampling rate of 25Hz. Considering the very low velocity of the oil-film flow, a large time interval is needed for achieving a relatively larger disaplacement of the oil pigment in order to obtain a better correlation in the later stage.

Therefore, every other 4 images was chosen as an image pair for the purpose of cross-correlations. This gives a time separation between image pairs of 0.16 second.

Before the cross-correlation analysis, image pairs have to be generated and go through a pre-processing procedure, which includes convert these 24bit colour images into 8 bit gray scale images, and an image ehancement process using Matlab standard functions. The contrast-limited adaptive histogram equalization algrithom enhances the contrast of the grayscale image to avoid amplifying any noise that might be present in the images.

The cross-correlation of the image pairs was conducted through using TSI Insight 3G^{TM} software. Applying 50% overlap, recursive Nyquist grids were used with the starting rectangular spot of 40×80 pixel and final spot of 10×20 pixel. Besides, the zero pad masks were used to remove large displacement aliasing, and also increased signal-to-noise ratio. Furthermore, the direct correlator was chosen to compute the correlation map between the two integration spots for a better accuracy although it took longer time to process than the commonly used FFT algorithm. Finally, the bilinear peak algorithm was used to locate the peak in the correlation map with sub-pixel accuracy by fitting a set of linear function to the highest pixel and its 4 nearest neighbours. This is helpful for very slow movement of the oil pigment in this visualisation. This process produced velocity fields with a spatial resolution of 7 mm in the streamwise direction and 3.5mm in the spanwise direction.

A serial of post-processing procedures, including a range validation filter and three-standard-deviation filter in time domain, were implemented to remove invalid vectors before obtaining final results. In the following section, the time-averaged velocity fields and their fluctuations will be discussed and compared with flow visualisation.

4. Results and discussion

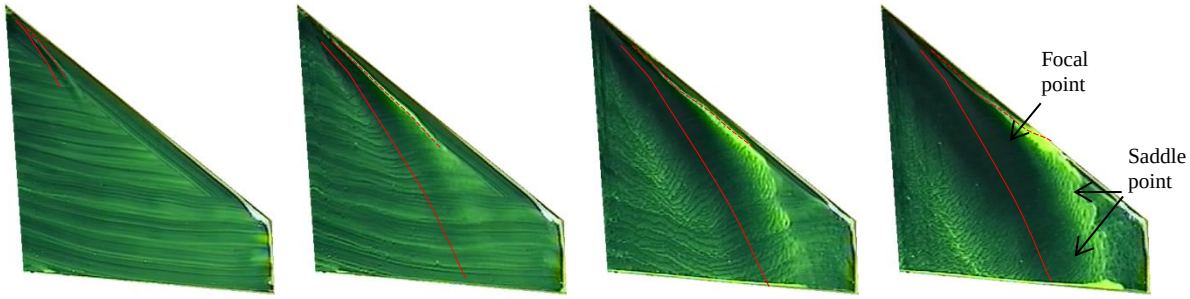

(a) (b) (c) (d)

Figure. 2: Snapshots of instantaneous flow visualisation for the wing model at α =9° and Re = 4.2×10^5 (a) 2s, (b) 6s, (c) 10s, (d) 14s (solid line: reattachment; dash line: Separation)

Figure 2 shows four snapshots extracted from the live video of the flow visualisation on the model surface at incidence angle α =9°. Figure 2a shows that the flow initially separated from the leading edge inboard of 30% of the semi-span and formed the leading edge vortex, and then reattached near to leading edge while the flow remained fully separated from the leading edge without any reattachment outboard of 30% of the semi-span, which was caused by the low free-stream velocity when starting the wind tunnel.

As the speed of the wind tunnel picks up, the reattachment zone extends up to 60% of the semi-span, and the secondary separation line moves closer to the leading edge, as indicated by the accumulated oil pigment and dash lines in Figures 2b to 2d. After the wind tunnel reaches the constant speed of 20 m/s, the flow pattern over the wing surface becomes steady. Firstly, oil pigment accumulated at the focal point near the leading edge at 50% of the semi-span, and was lifted from the wing from there. Secondly, it is also easy to observe the two saddle points at the wing tip region from the video image in Figure 2d.

Figure 3 shows the surface skin friction lines generated by the time-averaged cross-correlation velocity data superimposed on a flow visualisation image. It is seen that the skin friction lines were coincidenced with the

secondary separation line at the leading edge, which forms the leading edge separation bubble, as seen in Figure 2d. Furthermore, the bifurcation line corresponds the reattachment from flow visualisation at inboard of 50% of the semi-span, while the reverse flow was clearly identified by the upwards skin friction lines at outboard of 80% of the semi-span.

Figure 4 shows the contours of time-averaged velocity for the streamwise and spanwise components. The maximum spanwise component occurs at the spanwise positon of 0.7b while the streamwise component is small. A relative large streamwise component was identifed inboard of 60% of the semi-span, which indicate a high shear stress caused by the turbulent reattachment. Reverse flow mainly located at the wing tip and the region near the leading edge of the wing model. This features are attribute the leading edge vortex and complex interactions between the vortex system at the wing tip region.
To validate the data generated by this techniqe, a comparison was made between these velocity data and the time-averaged velocity field measured using three-componet LDA system at just 0.2 mm above wing [9]. Due to the high viscosity (over 10^2 - 10^4 times that of air) of the oil-film, the velocity has a far lower magnitude than that of the air flow velocity near the surface, even at 0.2 mm close to the wall. However, the flow directions should be consistant for air and oil-film flow since they both follow surface skin friction line except for some specail occasions, such as very thick oil flow region. It can be seen from Figure 5 that overall velocity vectors are matched each other very well between flow visualisation correlations data and LDA measurements at 0.2 mm close to the wall. For example, the average defference of the flow directions between those data sets are less than 2 degree for inboard of 50% of the semi-span. Slight discrpancies can be identified at the leading edge of the wing model and wing tip region. This is attibute to the complex flow patterns and thickness of the oil-film in the low flow region. In the leading edge, narrow separation bubble and perspective views of images make the cross-corretions unreliable while relative low amplitude velocity of oil-film flow make it difficute to estimated at the subpixel scale for the flow at the wing tip region.

Figure 6 shows the generated surface skin friction lines superimposed onto the contours of velocity of oil pigment over the wing surface at six incidence angles and $Re = 4.2\times10^5$. Figure 6a, obtained for incidence angle $\alpha = 4°$, shows straight skin friction lines across the middle section of the half-wing while the colour contours reveals that these lines cross two different flow regions, i.e. laminar attachment and turbulent reattachment. Turbulent reattachment produces a larger skin friction which produces a larger velocity of oil pigment in the yellow triangle region near the trailing edge. Figures 6b show the reattachment bifurcation line parallel to the leading edge which is identical to the oil flow visualisation. The typical flow patterns of 60° show relatively simple topologies observed for this slender wing. At incidence of 9°, no clear flow separation can be identified while typical twin vortical structures are clear in figure 6d, which shows reattachment lines and secondary separation line near the leading edges.

5. Conclusion

When the static images are not sufficiently clear to show the movement of the oil pigment, cross-correlation between nearby video frames can be carried out to produce the velocity vector field over the surface. The results show that the local skin friction directions agree well with LDA measurements and magnitude of velocity data shows difference levels of skin friction over the wing models.

Uncertainty of the measurements was related with the quality of the images and their resolution. Also, it is directly related to the local flow structures over the curved surface. Regarding to the speciality of the oil-film flow, the timing is also an important factor since the oil flow could not be constantly supply onto the surface once it was blown away. The density and thickness of the mixture are varied with time in the process of formation of the final flow topology. To obtain sensible data, all these factors need to be considered.

In the future, a higher resolution image system will be employed for the oil flow visualisation to resolve the detailed flow structures over swept wing model. Image enhancement algorithms could be helpful in improving the quality of the images and increasing signal-to-noise ratio. Besides, algorithms of cross-correlation, locating the peak of correlation were vital for the accuracy of the estimation of local velocity.

Acknowledgements

The authors wish to thank their academic and industrial partners in this MSTTAR Defence Aerospace Research Project. Funding for MSTTAR was provided by the EPSRC and the Ministry of Defence.

References

[1] Haines AB (1954). Some notes on the flow patterns observed over various swept-back wings at low Mach numbers. R&M No. 3192

[2] Hall IM and Rogers EWE (1960a). The flow pattern on a tapered sweptback wing at Mach number between 0.6 and 1.6 Part I, Aeronautical Research Council R&M No. 3271

[3] Hall IM and Rogers EWE (1960b). Experiments with a tapered sweptback wing of warren 12 platform at Mach number between 0.6 and 1.6 Part II, Aeronautical Research Council R&M No. 3271

[4] Lu, F K (2010). Surface oil flow visualization. The European Physical Journal-Special Topics, 182(1), 51-63.

[5] Tanner, LH, & Blows, LG. (1976). A study of the motion of oil films on surfaces in air flow, with application to the measurement of skin friction. Journal of Physics E: Scientific Instruments, 9(3), 194.

[6] Liu, T (2013). Extraction of skin-friction fields from surface flow visualizations as an inverse problem. Measurement Science and Technology, 24(12), 124004.

[7] Délery JM, Robert Legendre and Henri Werlé: towards the elucidation of three-dimensional separation. Annu. Rev. Fluid Mech. 2001. 33: 129-54

[8] Turner JT and Zhang S (2007) "Experimental study of the flow over a highly swept wing", Final report on MSTTAR DARP – GR/S 27443/01

[9] Zhang S, Jaworski AJ, Turner JT, and Wood NJ (2011) "Investigation of the three-dimensional flow over a 40° swept wing", Aeronautical Journal 115, Issue: 1169: 441-449

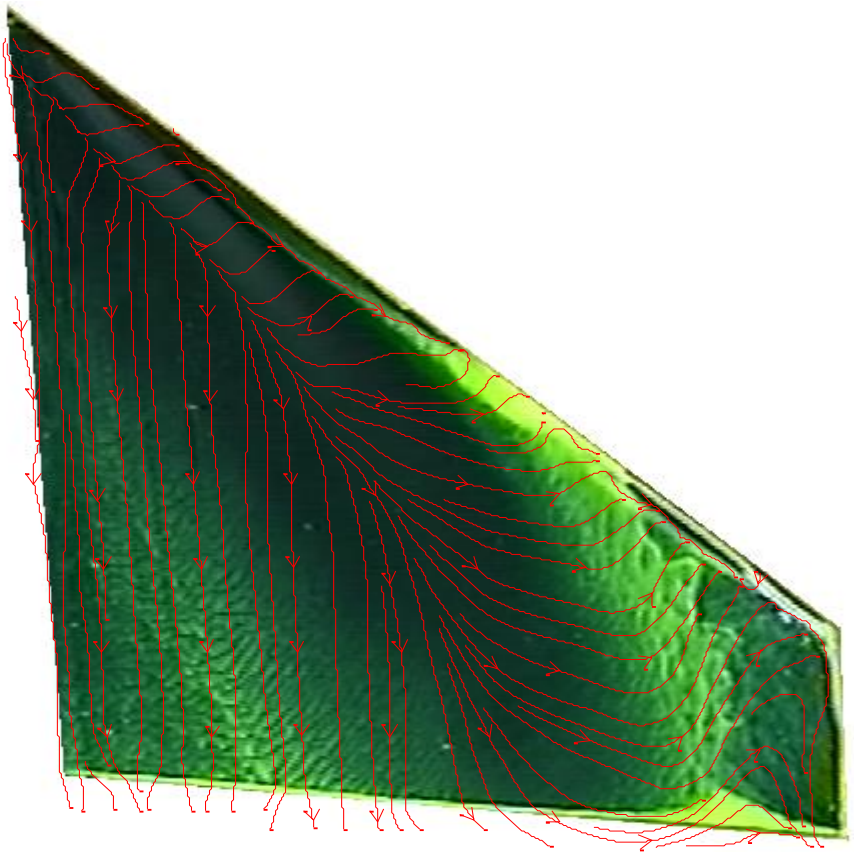

Figure. 3: Surface skin friction lines of the oil-film flow on the 40° wing model at α =9° and Re = 4.2×10^5

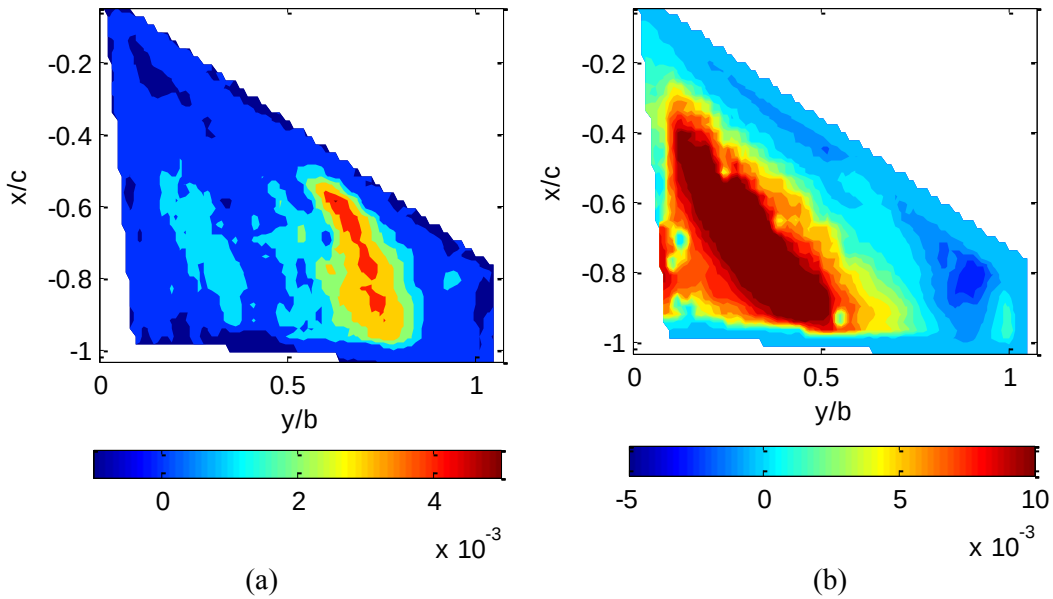

Figure. 4. Velocity contours of the surface oil-film flow on the 40° swept wing model at α =9° and Re = 4.2×10^5. (a) spanwise; (b) streamwise

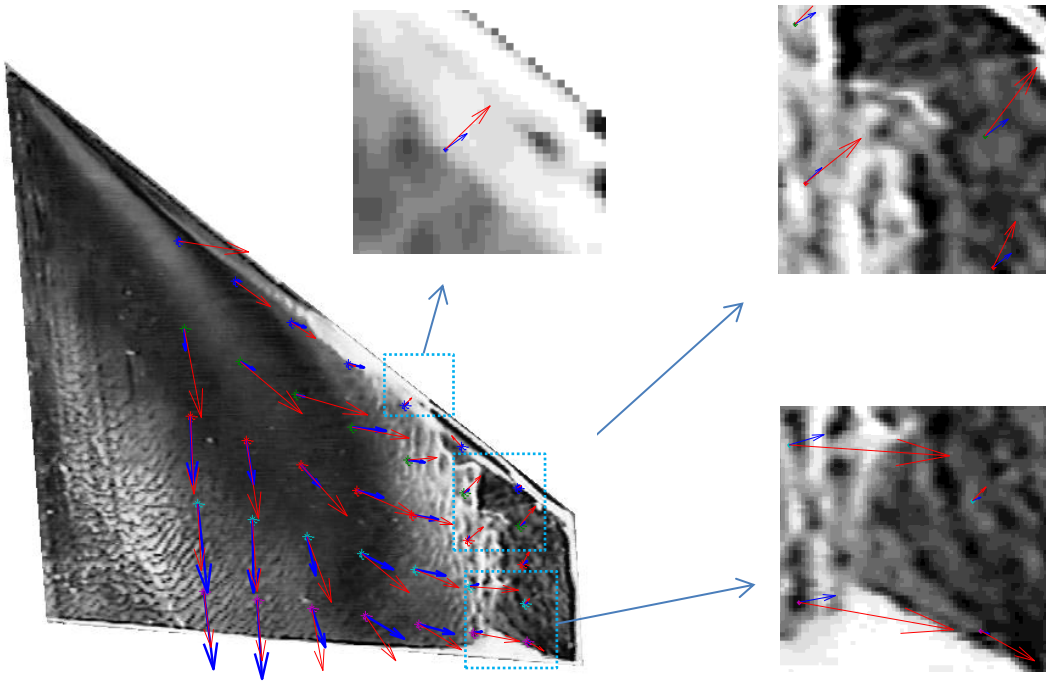

Figure. 5: A visual comparison between the time-averaged velocity vector field (red) measured using LDA at just 0.2 mm above the 40° wing surface with the surface flow direction (blue) yielded by the cross-correlations of visualisation images.

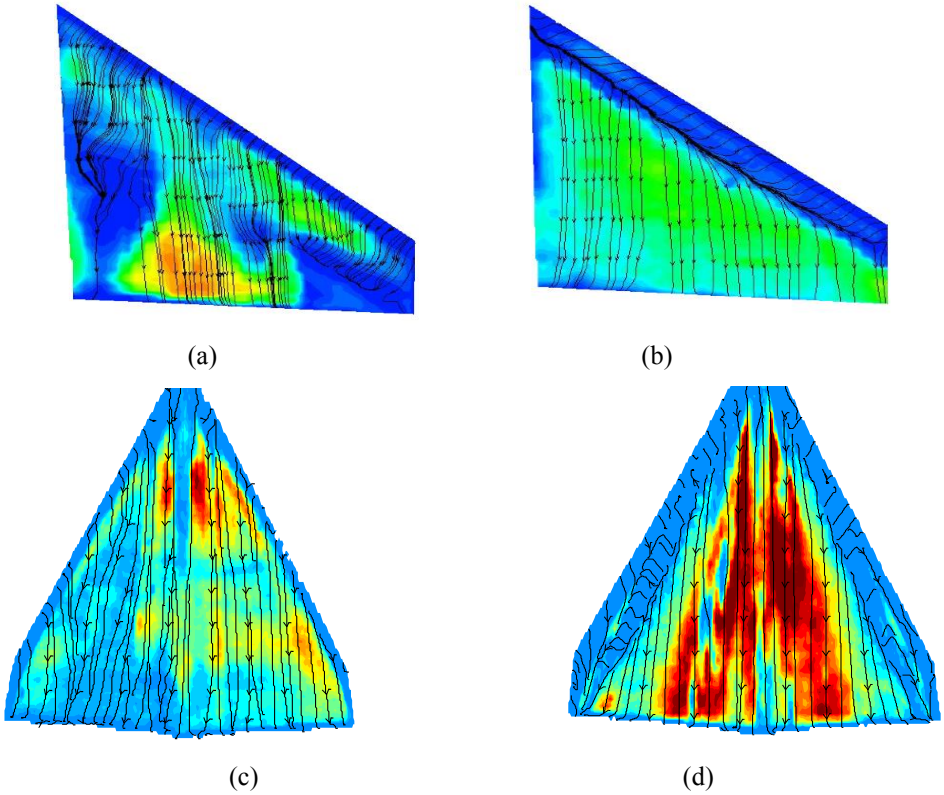

(a) (b)

(c) (d)

Figure. 6: The skin friction lines with the magnitude over swept wing models at different incidences (a) 4°, (b) 6°, (c) 9°, (d) 15°